Current Status of Research on the Oxidation Behavior of Refractory High Entropy Alloys

Bronislava Gorr, Steven Schellert, Franz Müller, Hans-Jürgen Christ, Alexander Kauffmann, and Martin Heilmaier**

Refractory high entropy alloys (RHEA) are considered as novel promising high-temperature materials for structural applications at ultrahigh temperatures primarily due to their attractive mechanical properties. By contrast, the oxidation behavior of RHEA has raised concern owing to pest oxidation, significant weight changes, scale spallation, or even complete oxidation at elevated temperatures. Herein, the currently available literature on high-temperature oxidation behavior of RHEA is reviewed with respect to alloy composition, mass changes, corrosion products, and scale constitution. While many RHEA indeed suffer from poor oxidation resistance similar to that of pure refractory metals, some RHEA exhibit very good protectiveness, which is attributed to the formation of either well-known protective scales such as α-Al_2O_3 or rarely encountered complex oxides such as $CrTaO_4$. Thermodynamic and kinetic aspects of oxide formation and growth are discussed to understand the oxidation mechanisms typical of RHEA. Further research directions with respect to additional in-depth studies elucidating the oxidation mechanisms as well as the further consequent improvement of the oxidation resistance of RHEA are developed from the current intermediate stage of research in the field.

1. Introduction

There is a perpetual need for increased operation temperatures (>1200 °C) in combustion engines such as gas turbines to enhance their energy efficiency.[1] While currently used Ni-based superalloys operate at their limit given by the solvus temperature of the precipitate γ' phase, the need for new high-temperature structural materials has been recognized for decades. Refractory metals (RM) and alloys have always been considered for future high-temperature structural applications primarily due to their high melting or solidus temperatures. In the classical definition, RM are elements with a body centered cubic (bcc) crystal structure (W prototype) that possess melting points above 2000 °C. **Table 1** summarizes some relevant properties of RM such as 1) density; 2) melting point; 3) ductile to brittle transition temperature (DBTT); 4) Young's modulus; 5) coefficient of thermal expansion; and 6) mass change after 8 h oxidation at 900 °C. An important benefit of RM is that they retain attractive high strength levels at elevated temperatures,[2] which is related to their high melting temperatures (see Table 1). On the contrary, RM exhibit several severe drawbacks that prevent their practical use as structural high-temperature materials so far. Some RM, e.g., W and Ta, possess very high densities, see Table 1, making their alloys virtually impossible for parts moving at high velocities. In addition, as Table 1 also demonstrates, some RM, in particular Mo and W, suffer from high DBTT. A further major disadvantage of RM across the board is their poor high-temperature oxidation resistance in environments with high oxygen activities. Depending on the temperature and atmosphere, RM form either porous and fast growing oxides or volatile oxides. Hence, complex oxidation kinetics due to superposition of positive contributions by solid scale growth and negative contributions by volatization, evaporation, or spallation occur.[3] A peculiar effect is the so-called "pesting" phenomenon, i.e., the fast disintegration of the metallic substrate due to intergranular oxidation, which can occur at already moderate temperatures of 600–800 °C.[4]

This article reviews the current status and progress in the field of refractory high entropy alloys (RHEA) with respect to their high-temperature oxidation resistance. Main emphasis will be placed on the oxidation resistance in air. We further define RHEA, such that they need to contain at least one element from Table 1, irrespective of the alloy microstructure. In accordance with the definition of high entropy alloys (HEA), RHEA are consequently defined in this review to have at least five metallic elements, each of which has an atomic percentage between 5% and 35%.[5] Furthermore, the impact of microalloying with Si or

Prof. B. Gorr, Dr. A. Kauffmann, Prof. M. Heilmaier
Institut für Angewandte Materialien
Karlsruhe Institut für Technologie (KIT)
Engelbert-Arnold-Str. 4, 76131 Karlsruhe, Germany
E-mail: bronislava.gorr@kit.edu; martin.heilmaier@kit.edu

S. Schellert, F. Müller, Prof. H.-J. Christ
Institut für Werkstofftechnik
Universität Siegen
Paul Bonatz Str. 9-11, 57068 Siegen, Germany

The ORCID identification number(s) for the author(s) of this article can be found under https://doi.org/10.1002/adem.202001047.

DOI: 10.1002/adem.202001047

Table 1. Some relevant properties of RM.

Property	Nb	Ta	Mo	W
Density ρ [g cm^{-3}]	8.57[54]	16.65[54]	10.28[54]	19.25[54]
Melting point T_m [K]	2741[54]	3269[54]	2893[54]	3695[54]
$0.5 \cdot T_m$ [K]	1371[54]	1635[54]	1447[54]	1848[54]
DBTT [°C]	−120[2]	−195[2]	30[2]	340[2]
Young's modulus [GPa]	103[54]	186[54]	320[54]	407[54]
Coefficient of thermal expansion [10^{-6} K^{-1}]	7.3[54]	6.3[54]	4.9[54]	4.5[54]
Mass change after 8 h oxidation at 900 °C [mg cm^{-2}]	185[53] (air)	120[53] (air)	−4080[39] (0.1 atm O_2)	4000[53] (air)

reactive elements on the oxidation behavior will also be addressed. To understand the underlying mechanisms and the role of particular elements, many studies have systematically investigated subsystems. The results of such studies will also be considered here as they contribute to the fundamental understanding of the oxidation behavior of RHEA and reveal a link to conventional alloys. Most of the alloys studied in this review were manufactured by arc melting. Some were processed by powder metallurgical methods. In many cases, high-temperature annealing processes were applied, in some cases in conjunction with isostatic pressing. Consequently, the microstructures under consideration reveal substantial variations with respect to the appearance and distribution of secondary phases. While the authors are aware of the significance of the microstructural mockup to oxidation resistance, we focus on the chemical composition in this review of the current status of research as the primary contribution to oxidation behavior.

2. Results

This section is structured in two parts. First, to put the research on developing oxidation resistance of RHEA into perspective, we introduce essential information on the oxidation behavior and the ability of the RM listed in Table 1 to form commonly accepted protective scales such as Cr_2O_3, Al_2O_3, and SiO_2 by the additions of Cr, Al, and Si to RM-based alloys and intermetallic compounds. These are fundamental for most of the RM-based HEAs development dealt with in this review. Second, we focus on the oxidation behavior of RHEA as well as their subsystems.

2.1. Oxidation Behavior of RM, RM-Based Alloys, and Intermetallic Compounds

The generally rather poor corrosion resistance of RM listed in Table 1 has manifold reasons, most notably: 1) low melting and/or vaporization temperatures of their oxides (see Table 1 and Table 3); 2) high growth and oxidation rates of the oxide scales (see Figure 7); 3) unfavorable ratio of the volume differences between the oxide and the metal from which it forms (see Table 6); and 4) significant gas solubility in RM (see Table 4). How strong each of the aforementioned aspects or a combination of them appears during oxidation heavily depends on the individual properties of the corresponding RM, its oxide(s) as well as the relative environmental conditions. Many attempts to improve oxidation resistance by alloying with potentially passivating Cr, Al, or Si were undertaken in the past decades. In general, thin (to avoid spallation), continuous (to provide passivation) Cr_2O_3 or Al_2O_3 scales were not observed on binary Mo–W-, Nb-, and Ta-based alloys (with a RM as the single main principle element or solid solution of them) with Cr or Al additions.[6–8] Even the increase in the content of these three potentially passivating elements to atomic fractions well above 50 at% was mostly unsuccessful or even led to deterioration of oxidation resistance. In some cases, though, more complex alloy compositions with third elements exhibited continuous Cr_2O_3 layers, for example, Pd in Mo–17Cr (wt%).[9]

By far the most research activities were performed on Si in binary or multinary alloys with RM, especially Mo[9] and Nb[10] as main principal element due to other necessary consideration for structural applications such as low temperature ductility and density. Si exhibits rather low solubility in RM-based solid solutions.[11–14] The dissolved Si contents are significantly below sufficient concentrations to form continuous SiO_2 scales. Hence, in-depth characterization focused on high Si containing materials with rather high fractions of RM silicides,[11–14] intermetallic compounds such as Mo_3Si, Mo_5Si_3,[15] and eventually $MoSi_2$.[16] For most of these silicides, still no continuous SiO_2 scales were observed especially not in the critical pesting regime. Further additions, such as B in the case of Mo–Si alloys, were necessary and have proved successful to modify oxide scale properties. In this specific case, the borosilica scale exhibits rather low viscosity, which enhances surface wetting of critical microstructural constituents such as the RM solid solution.[15]

Hence, Cr, Al, and Si, in general, improve the oxidation resistance of RM. However, in contrast to Ni-based alloys that exhibit protective oxide scales Cr_2O_3,[17] Al_2O_3,[18] and SiO_2[19] even in corresponding binary systems Ni–Cr, Ni–Al, and Ni–Si, more elaborated alloy compositions are required to provide reliable oxidation protectiveness to RM especially if protective Cr_2O_3 or Al_2O_3 is targeted. The simultaneous addition of Cr and Al to RM sometimes causes inferior oxidation behavior, in contrast to Ni–Cr–Al alloys in which Cr and Al act synergetic.[20]

Recently introduced RHEA possess a priori complex and sometimes unconventional chemical compositions, which allow to anticipate unexpected outcomes in the field of high-temperature corrosion behavior of RM-based alloys. As none of the constituents act as a principle element, the refractory elements might not dictate the fundamental oxidation properties as in the cases described earlier.

Table 2. Oxidation behavior of RHEA (literature data).

Alloy composition	Temperature, [°C]	Duration, [h]	Mass change, [mg cm^{-2}]	Corrosion products	Reference
$NbCrMo_{0.5}Ta_{0.5}TiZr$	1000	100	120	Cr_2O_3, $CrNbO_4$, Cr_2TiO_5,$Cr_2Ti_5O_{13}$	[21]
$NbCrMoTiAl_{0.5}$	1300	20	150	$(Ti,Cr,Nb)O_2$, Al_2O_3	[34]
$NbCrMoVAl_{0.5}$	1300	20	350	$CrNbO_4$, $CrVNbO_6$, V_2O_5, VO_2, Al_2O_3	[34]
$NbCrMoTiVAl_{0.5}$	1300	20	260	$(Ti,CrNbV)O_2$, Al_2O_3	[34]
$NbCrMoTiVAl_{0.5}Si_{0.3}$	1300	20	185	$(Ti,CrNbV)O_2$, Al_2O_3	[34]
WMoCrTiAl	1000	40	8	Rutile (TiO_2), $Al_2(WO_4)_3$ corundum (Cr_2O_3,Al_2O_3),	[55]
NbMoCrTiAl	900, 1000, 1100	48	1 (900 °C), 9 (1000 °C), 8 (1100 °C)	Rutile (TiO_2), corundum (Cr_2O_3,Al_2O_3) (1000 °C)	[35]
NbMoCrTiAl1Si	900, 1000, 1100	48	5 (1000 °C)	Rutile (TiO_2), corundum (Cr_2O_3,Al_2O_3) (1000 °C)	[35]
TaMoCrTiAl	500, 900–1100, 1300–1500	12–300	0.4 (900 °C, 48 h), 3.5 (1000 °C, 300 h), 10 (1500 °C, 12 h)	TiO_2, Al_2O_3, Cr_2O_3, $CrTaO_4$ (1000 °C)	[262935]
TaMoCrTiAl1Si	900, 1000, 1100	48	0.6 (900 °C), 1.2 (1000 °C), 3.7 (1100 °C)	TiO_2, Al_2O_3, Cr_2O_3, $CrTaO_4$ (1000 °C)	[56]
NbTiZrV	1000	100	Completely oxidized after 8 h	$TiNb_2O_7$, TiO_2, $Nb_2Zr_6O_{17}$, V_2O_5	[43]
NbTiZrCr	1000	100	100	$NbCrO_4$	[43]
TiZrNbHfTa	700, 900, 1100, 1300	100	Pesting (700 °C, 75 h), completely oxidized (1300 °C)	Complex mixed oxides	[24]
$Al_{0.5}TiZrNbHfTa$	700, 900, 1100, 1300	100	13 (700 °C), completely oxidized (1300 °C)	Complex mixed oxides	[24]
AlTiZrNbHfTa	700, 900, 1100, 1300	100	10 (700 °C), completely oxidized1300 °C)	Complex mixed oxides	[24]
AlNbTiZr	600–1000	3, 50	2.5 (600 °C, 3 h), 14 (1000 °C, 3 h)	$AlNbO_4$, Ti_2ZrO_6, TiO_2, Ti_2O_3, ZrO_2, Al_2O_3, NbO (1000 °C)	[57]
$Hf_{0.5}Nb_{0.5}Ta_{0.5}Ti_{1.5}Zr$	600-1100	5	Pesting (600–1000 °C), 0.38 (1000 °C), ≈0 (1100 °C)	$(Ti_{1.5}Ta_{0.5}Nb_{0.5}Hf_{0.5}Zr)O_8$, $NbZrO_{17}$, Nb_2TiO_7 (1100 °C)	[25]
Al20Cr10Mo10Nb20Ti20Zr20	1000	20	21	–	[27]
Al30Cr10Nb20Ti20Zr20	1000	20	20	$ZrTiO_4$, $CrNbO_4$, $AlNbO_4$	[27]
Al10Cr30Nb20Ti20Zr20	1000	20	39	–	[27]
$AlNbTiVZr_{0.25}$	600–900	100, 50 (900 °C)	7 (600 °C, 100 h), 220 (900 °C, 50 h)	$TiNb_2O_7$, $AlNbO_4$, $Nb_2Zr_6O_{17}$ (900 °C)	[58]
CrMoNbTaV	900–1100	25	33 (900 °C), 43 (1000 °C), 10 (1100 °C)	Nb_2O_5, NbO_2, $CrTaO_4$, Ta_9VO_{25}, Nb_9VO_{25}, TaO, $CrNbO_4$ (1000 °C)	[59]
Al20Nb30Ta10Ti30Zr10	1000	100	50	$NbAlO_4$, ZrO_2, $Ti_7Al_2O_{15}$, $Ta_2Nb_4O_{15}$, TiO_2	[28]
Al20Cr25Nb20Ti20Zr15	800	24	21	TiO_2, NbO, Al_2O_3, ZrO_2, $ZrTiO_4$, $CrNbO_4$	[60]
Al20Cr25Nb19Ti20Zr15Y1	800	24	9	TiO_2, NbO, Al_2O_3, ZrO_2, $ZrTiO_4$, $CrNbO_4$	[60]
13.4Ta20.3Mo15.2-Nb25.2Cr5.4Ti17.6Al2.9Si	1000–1400	100, 200	6.5 (1000 °C, 200 h), 18 (1400 °C, 100 h)	$CrTaO_4$, Cr_2O_3, Al_2O_3, mullite @1400	[30,31]
NbZrTiCrAl	800, 1000, 1200	50	10 (800 °C) 50 (1000 °C) 180 (1200 °C)	$CrNbO_4$, ZrO_2, TiO_2, Al_2O_3, $ZrNbO_7$ (1000 °C)	[61]
$Nb_{1.3}Si_{2.4}Ti_{2.4}Al_{3.5}Hf_{0.4}$	800, 1200	100	0.7 (800 °C) 1.5 (1200 °C)	$(Ti_{0.95}Nb_{0.048})O_2$, $(Ti_{0.95}Nb_{0.95})O_4$, HfO_2, $TiNb_2O_7$, Nb_2O_5, TiO_2, SiO_2, $TiAl_2O_5$, α-Al_2O_3 (1200 °C)	[32]
TaMoCrAl	1000	100	Completely oxidized	Cr_2O_3, Al_2O_3, $CrTaO_4$, Ta_2O_5	[26]

Table 2. Continued.

Alloy composition	Temperature, [°C]	Duration, [h]	Mass change, [mg cm^{-2}]	Corrosion products	Reference
NbMoCrAl	1000	100	Completely oxidized	Cr_2O_3, Al_2O_3, Nb_2O_5, TiO_2	[26]
NbCrVWTa	600, 800–1000, 1200, 1400	24	140 (800 °C) 320 (1000 °C) 300 (1400 °C)	Nb, Cr, V, and W oxides, Ta oxides (1200 °C)	[62]
Al10CrNbTiZr10	1000	50	24	$CrNbO_4$, Al_2O_3, $AlTiO_5$	[63]
NbMoCrTiAlTY	1000	48	25 (1000 °C)	TiO_2, Al_2O_3, Cr_2O_3, Nb_2O_5, $CrNbO_4$, $YNbO_4$ (1000 °C, 24 h)	[46]
TaMoCrTi	1000	5	0.9	TiO_2, $CrTaO_4$, $MoTiTa_8O_{25}$	[33]
TaMoTiAl	1000	5	2.5	Al_2O_3, TiO_2, $MoTiTa_8O_{25}$	[33]
TaMoTi	1000	5	22	TiO_2, $MoTiTa_8O_{25}$	[33]

2.2. Oxidation Behavior of RHEA

Table 2 compiles the results on the oxidation behavior in air of a broad variety of RHEA by the definition given in the introduction. It shows that the oxidation behavior of RHEA has been studied in a wide temperature range from 500 to 1500 °C of which the majority of research focusing on 1000 °C. Besides, the oxidation times vary extremely from 5 up to 300 h. In cases where more than one temperature was given, the values of the mass change at the lowest and the highest test temperatures are listed. Also, Table 2 indicates whether some alloy pests at a particular temperature. Table 2, however, does deliberately not include oxidation rate constants, because several prerequisites for a serious analysis are not fulfilled in a vast majority of the studies reviewed. First, sufficiently long (at least 24 h) oxidation experiments should be performed to guarantee that oxidation rate constants are calculated using data from the steady-state oxidation stage. Second, oxidation rate constants calculated using exclusively thermogravimetric data will be false if RHEA contain elements that form liquid or volatile oxides. Therefore, this calculation should either consider the contribution of these weight losses and/or should be verified by the values of the scaling constants by adequate microstructural analyses. This issue is quantitatively exemplified in the following (see Figure 2).

Figure 1 compiles recorded mass changes of those RHEA only who were studied for at least 20 h at 1000 °C. These data were collected from the manuscripts cited in Table 2. Consequently, RHEA, which were oxidized at temperatures other than 1000 °C or for times shorter than 20 h, are not included in Figure 1. The comparison reveals that Zr- and V-containing alloys exhibit the highest mass gain indicating poor oxidation performance. A significant decrease in mass change, which usually comes along with an enhancement of the oxidation protectiveness, is clearly recognized if Cr and Al were added to RHEA. The lowest mass changes and, consequently, the highest oxidation resistance after 20 h oxidation at 1000 °C exhibit alloys

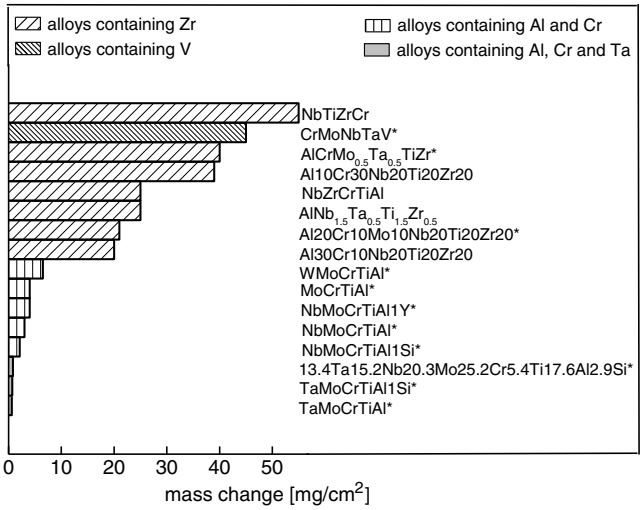

Figure 1. Comparison of mass changes of different RHEAs oxidized at 1000 °C for 20 h; alloys with possibly uncorrected values of mass change due to the formation of gaseous Mo and/or V oxides are denoted by asterisks.

Table 3. Properties of RM oxides relevant for RHEA.

Metal	Oxide	Oxide properties
V	V_2O_5	Melts above 675 °C[2]
Mo	MoO_3	Evaporate above 795 °C[2]
W	WO_3	Evaporate above 1000 °C[2]
Nb	Nb_2O_5	Evaporate above 1370 °C[2]
Ta	Ta_2O_5	Evaporate above 1370 °C[2]

that contain Cr, Al, and Ta with the seemingly best oxidation performance demonstrated by the equiatomic alloy TaMoCrTiAl.

It should be pointed out here that the data of thermogravimetric analyses (TGA) are not an entirely reliable indicator to evaluate the oxidation resistance of RHEA as some RM form liquid or volatile oxide species even at temperatures below 1000 °C (see **Table 3**). To date, only few studies considered the effect of (simultaneous) oxide evaporation on the recorded values of the mass gain. The analysis of the oxide scale formed on the alloy NbCrMo0.5Ta0.5TiZr revealed that the oxide scale contains a reduced amount of Mo, i.e., about 56% less relative to the amount of the non-oxidized alloy. Assuming that MoO_2 forms at the test temperature of 1000 °C, the total weights of the escaped MoO_2 and, therefore, Mo were estimated to be 63.9 and 47.9 mg after 100 h of oxidation, respectively.[21] **Figure 2** demonstrates that evaporation of Mo oxides in the alloys within the system Ta–Mo–Cr–Ti–Al with different Ta contents can severely affect the absolute values of the mass change and may lead to dramatic misinterpretation of oxidation rates and, therefore, to draw false conclusions on acting oxidation

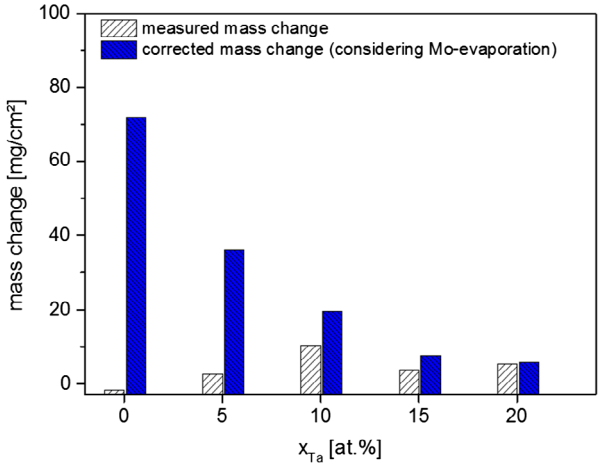

Figure 2. Measured and calculated values of mass change considering the Mo evaporation of RHEA within the system *x*Ta–Mo–Cr–Ti–Al ($x = 0$; 5; 10; 15; 20) during exposure to air for 24 h at 1200 °C. The basis for the calculation was the assumption that Mo completely escaped from the inward growing oxide scale. The original metal surface was determined using focused ion beam markers, which further allowed the determination of the volume of the inwardly grown oxide scale that is equal with the volume of the original alloy from which Mo was escaped by the formation of volatile MoO_3. The Mo fraction in the original alloy, i.e., 20 at%, was considered.

mechanisms. The mass changes measured by TGA (gray bars in Figure 2) suggest that the quaternary equimolar alloy MoCrTiAl exhibits a superior oxidation resistance compared with that of its quinary TaMoCrTiAl counterpart. The opposite trend appears if mass changes including consideration of the evaporation of Mo oxides are compared, black bars in Figure 2. The equiatomic quinary alloy TaMoCrTiAl then exhibits the highest oxidation resistance that is confirmed by microstructural analyses of the oxide scales formed on all alloys studied in the context of Figure 2. **Figure 3** shows that the oxide scale grown on the quinary TaMoCrTiAl alloy is substantially thinner and appears dense and compact, whereas poorly adherent and porous scales are found on the quaternary MoCrTiAl alloy apparently allowing for evaporation of Mo oxides, see the different scales in Figure 3a,b, respectively. The results presented earlier evidently demonstrate that any TGA data should be critically evaluated if vaporization of RM oxides cannot be excluded. To quantify the evaporation of RM oxides experimentally, TGA should, hence, always be coupled with mass spectrometry. Alternatively, a theoretical estimation of such contributions may be performed as, for example, described in the previous studies.[22,23]

Corrosion products and their manifestation strongly depend on the alloy composition and atmospheric conditions. Further characteristics such as phase constitution, impurities, and macroscopic defects such as cracks and porosity also affect the formation and growth of oxide scales. In terms of corrosion products observed in RHEA, the form of appearance can be classified into four types: 1) oxygen dissolution in metal and crack formation (**Figure 4**a); 2) thick non-protective scales (Figure 4b); 3) thin oxide layers and internal oxide/nitride precipitates (Figure 4c); and 4) highly protective oxide scales (Figure 4d).

In case of type 1), high oxygen solubility in the metallic material causes an extended oxygen diffusion zone (ODZ) together with severe crack formation, whereas the surface oxide layers (SOL) might spall off. Such oxidation behavior was observed, for example, in TiZrNbHfTa[24] and Hf0.5Nb0.5Ta0.5Ti1.5Zr.[25] The vast majority of RHEA oxidize according to type 2) and form thick oxide scales. In addition to simple oxides, such as TiO_2, Al_2O_3, V_2O_5, etc., numerous complex oxides, e.g., $NbCrO_4$ and $TiNb_2O_7$, were found in the oxide scale formed on RHEA (see Table 2).[21,26–28] Some RHEA seem to form thin oxide scales that provide significant protectiveness resulting in low values of the mass gain, type 3). The formation of continuous $CrTaO_4$ adjacent to the metal results in the formation of quite thin oxide scales. However, a pronounced zone of internal corrosion is usually detected below the $CrTaO_4$ layers.[26,29–31] Only one alloy oxidizes according to type 4). A fully continuous and protective Al_2O_3 scale was observed on the alloy $Nb_{1.3}Si_{2.4}Ti_{2.4}Al_{3.5}Hf_{0.4}$ after oxidation for 100 h at 1200 °C (see Figure 4d).[32]

Though some RHEA contain rather high concentrations of Cr up to 25 at%,[26,33] continuous Cr_2O_3 scales do not form on any of these RHEA. As mentioned earlier, only one alloy was reported to form a continuous Al_2O_3 scale. It should, though, be pointed out that semi-continuous Al_2O_3 scales were found on the alloys NbCrMoTiVAl0.5Si0.3[34] and TaMoCrTiAl.[35] As rather low concentrations of Si (below 5.7 at%) were added to some RHEA,[34] SiO_2 layers were commonly not found on these alloys. However, it is hypothesized that Si additions may promote the formation of other protective oxides such as Al_2O_3.[34,35]

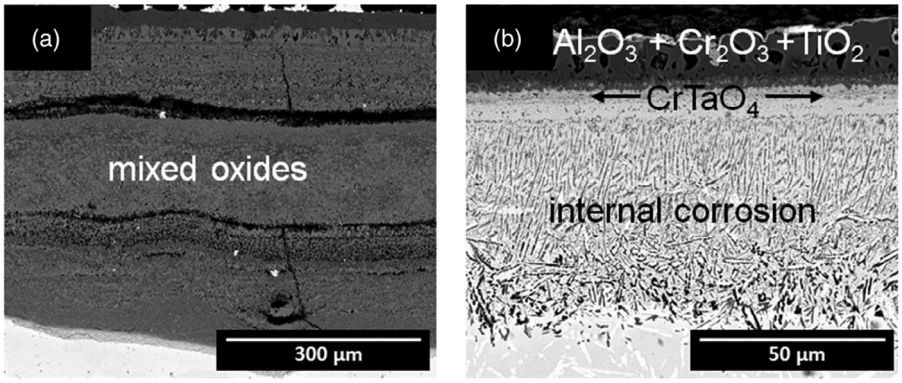

Figure 3. Oxide scales formed on two equiatomic RHEA after 24 h of oxidation at 1200 °C; a) MoCrTiAl and b) TaMoCrTiAl.

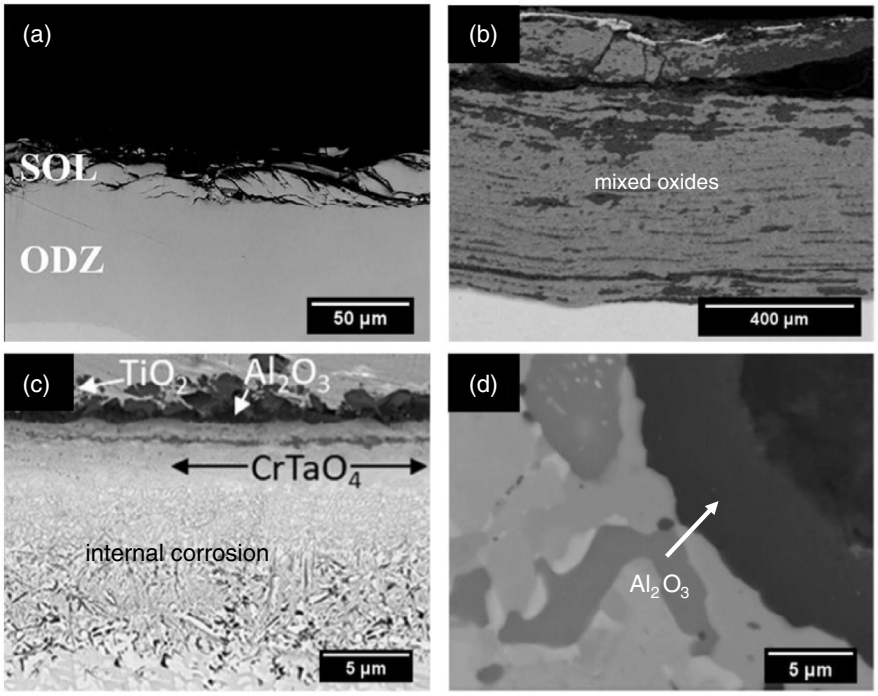

Figure 4. Cross sections of various RHEA after oxidation in air (conditions in brackets): a) surface oxide layer (SOL) of the alloy TiZrNbHfTa (1 h at 700 °C),[35] ODZ represents the oxygen diffusion zone. Reproduced with permission.[24] Copyright 2018, Wiley. b) Oxide scale formed on the alloy NbMoCrTiAl (100 h at 1000 °C)[21] (mixed oxides consists of Nb_2O_5, TiO_2, Cr_2O_3, Al_2O_3, and $CrNbO_4$). Reproduced with permission.[26] Copyright 2019, Elsevier. c) Backscattered electron (BSE) image of the alloy TaMoCrTiAl (100 h at 1000 °C).[21] Reproduced with permission.[26] Copyright 2019, Elsevier. d) BSE image of an α-alumina scale formed on the alloy Nb1.3Si2.4Ti2.4Al3.5Hf0.4 (100 h at 1200 °C).[28] Reproduced under the terms of the CC BY 4.0 license.[32] Copyright 2019, The Authors. Published by MDPI.

An unexpectedly high oxidation resistance, i.e., low values of the mass change and thin external oxide scales, was recognized for alloys that form complex oxide scales such as $CrTaO_4$. These scales were observed in the alloy systems Ta–Mo–Cr–Ti,[33] Ta–Mo–Cr–Ti–Al,[26,29] and Ta–Mo–Nb–Cr–Ti–Al–Si.[30] Though $CrTaO_4$, which possesses the rutile-type crystal structure, has not been known as a protective oxide in the past, it obviously possesses a potential to protect RHEA as a relatively low mass gain was measured even at 1500 °C.[29] **Figure 5**a reveals that the oxidation rate constants of the equiatomic alloy TaMoCrTiAl (red line and data) that is a $CrTaO_4$ former are comparable with those of commercially available Cr_2O_3- (black shaded area) and Al_2O_3-forming (green) Ni-based alloys.[29] To avoid possible superimposed effects from evaporating Mo oxides and scale growth of other oxides such as TiO_2 and Al_2O_3 on the oxidation rate constants calculated using thermogravimetric data, the thicknesses of $CrTaO_4$ scales were determined as a function of oxidation time in our very recent investigations. The results reveal that $CrTaO_4$ grows obeying a parabolic rate law indicating a slow growth process through solid-state diffusion of oxygen through the scale (see Figure 5b). The parabolic growth constants of $CrTaO_4$ are

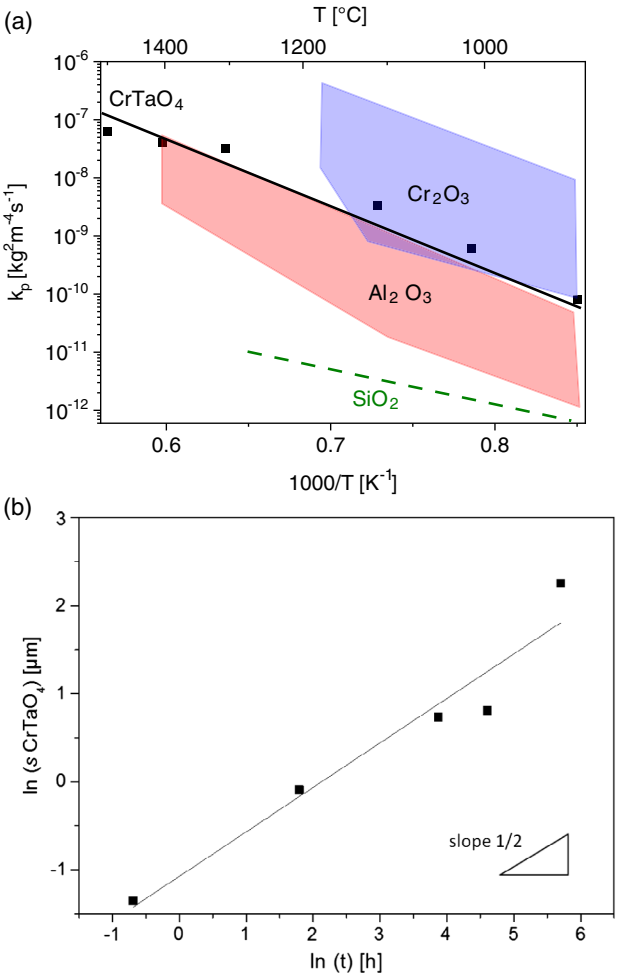

Figure 5. Growth rates of $CrTaO_4$ scales; a) oxidation constants of the alloy TaMoCrTiAl calculated using thermogravimetric data[29] and b) growth rates of the $CrTaO_4$ scale grown on the alloy TaMoCrTiAl at 1000 °C; *s* represents the scale thickness in µm.

given in Section 3.2, discussing kinetic aspects of oxidation behaviors of RHEA.

3. Discussion

Current research efforts to develop RHEA with high corrosion performance at elevated temperature are built on knowledge collected for materials with a single principle element and provide barely limited benefit to RHEA. To understand the peculiarities of the oxidation behavior of RHEA, a fundamental approach used for numerous conventional high-temperature materials will be carried out next, which includes studies of thermodynamics and kinetics in terms of the alloy response to aggressive environments at high temperatures.

3.1. Thermodynamic Aspects

Figure 6 compares the standard-free enthalpies of formation of oxides as a function of temperatures for RM and other high

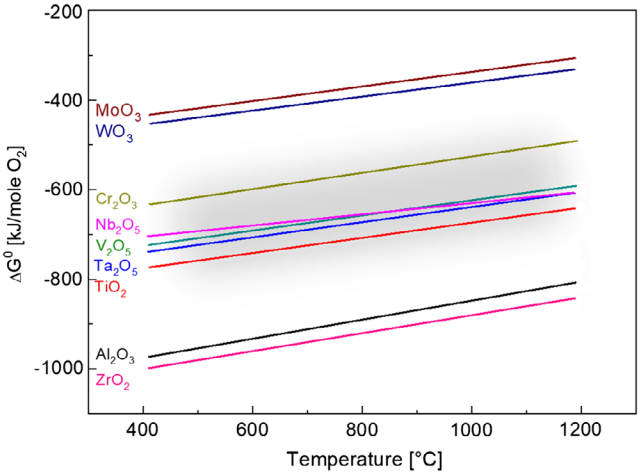

Figure 6. Thermodynamic stabilities of elements relevant for RHEA systems.[50]

melting elements relevant for this study (see Table 2). In addition, corresponding data of the Cr/Cr_2O_3, Ti/TiO_2, and Al/Al_2O_3 equilibria are also displayed in Figure 6 as Cr, Ti, and Al are often added to RHEA to improve the oxidation resistance and/or to reduce the alloy density. Apparently, oxides of many elements that are typically present in RHEA possess very similar thermodynamic stabilities. In particular, oxides enclosed in the gray-shaded area including Cr_2O_3, Nb_2O_5, V_2O_5, Ta_2O_5, and TiO_2 exhibit only marginal difference in the standard-free enthalpies of formation; for example, the difference between Cr_2O_3 and TiO_2 yields a value of only 160 kJ mol^{-1} O_2 at 1000 °C. In Cr_2O_3- or Al_2O_3-former Ni-based superalloys, however, the corresponding differences between NiO and Cr_2O_3 or Al_2O_3 amount to 265 and 590 kJ mol^{-1} O_2, respectively. Such pronounced differences in oxide stabilities facilitate the selective oxidation of Cr and/or Al in Ni-based superalloys. By contrast, oxides with similar thermodynamic stabilities tend to form simultaneously, finally resulting in the formation of a non-protective oxide mixture. This is what typically happens in RM-based alloys or intermetallic compounds (see Section 2.1) and RHEA (see Section 2.2). In line with these findings, also the similar thermodynamic stabilities of Al_2O_3 and TiO_2 (with the difference being only 170 kJ mol^{-1} O_2) lead to a concurrent growth of both oxides creating the formation of thick and non-protective mixed scales during oxidation of TiAl-based alloys,[36] hence limiting their current application to temperatures below 800 °C.

It is noteworthy in Figure 6 that Al and Zr form the most stable oxides, whereas Mo and W represent the most noble metals. It is, therefore, not surprising that Al and Zr oxides are always found as either simple or complex oxides if RHEA contain these elements (see Table 2). The relatively low thermodynamic stabilities of MoO_3 and WO_3, on the contrary, suggest that oxidation of Mo and W can be prevented if the formation of dense scales of less noble metals (such as Al) takes place.

The standard-free enthalpy of formation of complex oxides can be determined as suggested by Massard et al.[37] Müller et al.,[26] for example, calculated a value of −568 kJ mol^{-1} O_2 for $CrTaO_4$

at 1000 °C according to Equation (1) and (2). Considering the high thermodynamic stability of $CrTaO_4$ (with a standard-free enthalpy of formation below the one of Cr_2O_3) in addition to its low growth rates (see Figure 5), it may be hypothesized that $CrTaO_4$ can be protective in RHEA that contain Ta and Cr.

$$1/2Cr_2O_3(s) + 1/2Ta_2O_5(s) = CrTaO_4(s) \quad (1)$$

$$\Delta G_{CrTaO_4} = 1/2(\Delta G_{Cr2O_3} + \Delta G_{Ta2O_5}) = -568\,\mathrm{kJ\,mol^{-1}O_2} \quad (2)$$

It is well known that, besides, solid oxides RM can form gaseous and liquid oxides with sublimation temperatures that vary strongly (see Table 3). While V_2O_5 melts at a very moderate temperature of 675 °C, Nb and Ta form oxides that become gaseous at a substantially higher temperature of 1370 °C. The formation of liquid or volatile oxides may prevent the formation of dense scales or destroy the integrity of initially protective oxide layers, leading to so-called catastrophic oxidation.[38] Examining the alloys listed in Table 2, it can be concluded that all V-containing alloys show extremely high values of mass change that can probably be explained by the formation of liquid V_2O_5 inhibiting the formation of dense oxide scales. To exclude such dramatic implications, the sublimation temperature of all oxides relevant for a particular alloy should ideally be higher than the operation temperatures in a specific technical application.

The next severe shortcoming of RM is their susceptibility to interstitial (O, C, N, and H) contamination. Data for oxygen are given in **Table 4**. Only W and Mo dissolve negligible concentrations of oxygen, whereas other RM are prone to notable oxygen take up. Some RHEA, e.g., TiZrNbHfTa[24] (see Figure 4a), reveal pronounced zones enriched in oxygen. This unfortunate feature may strongly influence the oxidation mechanisms of RHEA, which will be described in the following.

3.2. Kinetic Aspects

As oxidation rates of pure RM are usually very high, fast metal consumption due to corrosion takes place. **Figure 7** displays the oxidation rates of selected RM, i.e., Ta, Nb, W, Zr, and Cr in the temperature range from 700 to 1100 °C. As both Mo and V form low melting oxides, see Table 3, oxygen consumption of these metals at 1000 °C is shown in **Figure 8**. It should be noted that all of the oxygen used forms volatile molybdenum trioxide at 1000 °C in case of Mo,[39] whereas solid VO_2 was observed in addition to the liquid V_2O_5 during oxidation of pure V.[40] To conclude, the high oxidation rates of RM account for remarkable values of the mass gain of many RHEA (see Table 2 and Figure 1). This is particularly evident in case of Zr-containing RHEA, which yield extremely fast oxidation kinetics (see Figure 1).

The thermodynamic issues discussed in the previous section reveal that the formation of protective scales such as chromia or alumina on RHEA is impeded by intrinsic thermodynamic driving forces, which could, though, be settled by kinetics aspects.

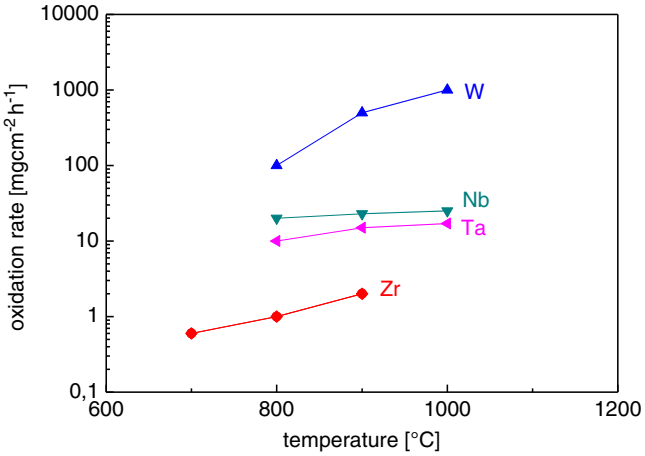

Figure 7. Oxidation rates of pure RM (Zr,[51] W,[52] Nb,[53] and Ta[53]) in the temperature range 700–1100 °C.

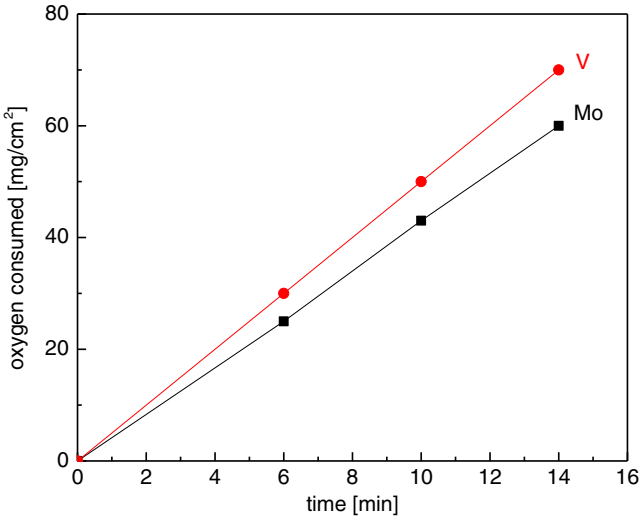

Figure 8. Oxygen consumption of Mo in 0.1 bar O_2[39] and V in air[40] at 1000 °C.

Possible mechanisms could be derived from less complex binary or ternary RM-based alloys, which were discussed in Section 2.1. For example, the addition of Pd seems to support the formation of chromia scales in some RM systems, e.g., Mo–Cr[9] and W–Cr alloys.[41] Mechanistically, Pd segregates to the grain boundaries of the W–29Cr (wt%) alloy providing easy diffusion channels for Cr to the surface that supports the formation of a compact chromia layer, at least temporarily.[41] Another possibility to accelerate the formation of protective oxide scales is the establishment of additional nucleation cites as has been demonstrated by the addition of 0.5 wt% Y to W–12Cr (wt%).[42]

Table 4. Oxygen solubility in pure elements at 1000 °C relevant for RHEA.

Element	W	[Nb]	Ta	Mo	V	α-Zr	β-Zr	α-Hf	α-Ti	β-Ti
O solubility, [at%]	0.03[64]	2.5[65]	3[66]	0.03[64]	3.2[67]	30[68]	1.5[68]	20[69]	14[70]	1[70]

Obviously, fast formation of compact oxide films, which separate the metallic substrates from the surrounding atmosphere, is a decisive prerequisite in terms of oxidation resistance of RM-based materials. If chromia, alumina, or silica cannot be realized on RHEA, alternative oxides may be considered. As described earlier, RHEA that form $CrTaO_4$ scales reveal unexpectedly high resistance against oxidation. The growth constant of $CrTaO_4$, calculated using the kinetic data for the equiatomic alloy TaMoCrTiAl at 1000 °C, lies in between those of protective chromia and alumina (see **Table 5** and Figure 5). This exciting finding confirms that $CrTaO_4$ may be considered as a promising oxide that can protect RHEA at high temperatures. Despite these perspective protective properties of $CrTaO_4$, the growth constant is twice as high as compared with that of Al_2O_3. In addition, relatively thick zones of internal corrosion were observed below $CrTaO_4$ layers indicating significant inward diffusion of oxygen and nitrogen. Furthermore, the properties of $CrTaO_4$ in atmospheres other than air are unknown so far.

3.3. Other Aspects

In addition to thermodynamic and kinetic aspects inhibiting selective oxidation of Cr and/or Al in RHEA containing significant amounts of these elements, other aspects may account for the inability of these alloys to form long-term protective scales. Growth stresses generated by the oxidation process in the oxide scales may lead to scale failure. Growth stresses developed during isothermal oxidation may arise from a number of reasons. In case of RHEA, the most relevant are: 1) compositional changes in the alloy; 2) oxide (trans)formation within the scale; and 3) volume differences between the oxide and the metal from which it forms. Compositional changes resulting in growth stresses by changes in the lattice parameter of the alloy occur if high amounts of oxygen are dissolved in RHEA. TiZrNbHfTa, for example,[24] seems to suffer from this shortcoming probably, because all elements are intrinsically prone to solve notable amount of oxygen (see Table 4). Chemical reactions between simple oxides that have been built simultaneously may lead to volume changes within the scale and, consequently, to normal stresses and the formation of cracks, pores, etc. Many researchers observed simple oxides during initial oxidation and the formation of complex oxides after prolonged oxidation. Butler et al.[43] reported, for example, the formation of TiO_2 and $TiNb_2O_7$ on NbTiZrV after 4 and 100 h of oxidation at 1000 °C, respectively. Chemical reactions between simple oxides may, on the contrary, have a positive impact as in case of the formation of continuous $CrTaO_4$ scales that effectively reduce the oxidation rate.[26,30] The formation of different oxide polymorphs may lead to notable anisotropic volume expansion and, thus, to crack formation. For example, various monoclinic and orthorhombic polymorphs have been observed for Nb_2O_5.[44,45] The overwhelming majority of RHEA include Nb primarily because of its attractive low density (see Table 1) and intrinsic ductility at ambient temperature. However, many of these alloys suffer from insufficient oxidation resistance (see Table 2 and Figure 1).

Table 5. Parabolic growth constants of oxides Al_2O_3, Cr_2O_3, and $CrTaO_4$ at 1000 °C.

Oxide	Oxidation constant k' [$m^2 s^{-1}$]
Al_2O_3	1.50×10^{-17} [71]
Cr_2O_3	8.08×10^{-17} [71]
$CrTaO_4$	3.83×10^{-17} [29]

Table 6. Oxide-Metal volume ratios (PBR) of metals relevant for RHEA.

Oxide	ZrO_2	Ta_2O_5	Nb_2O_5	V_2O_5	WO_3	TiO_2	Cr_2O_3	Al_2O_3
PBR	1.56[72]	2.5[73]	2.68[72]	3.19[73]	3.3[74]	1.78[72]	2.07[72]	1.28[72]

Finally, growth stresses may also arise from unfavorable values of the Pilling–Bedworth ratio (PBR) of corresponding metals and oxides. **Table 6** lists the PBR values for oxides relevant for RHEA systems. It is clear that Ta, Nb, V, and W oxides exhibit extremely high PBR values that will give rise to enormously high compressive stresses developed within the scales. However, such stresses would seem to be feasible if the oxide scale grows by inward diffusion of oxygen anions, while they might be acceptable if the scale grows due to outward cation transport. To determine whether the PBR should be considered, the oxidation mechanism should be identified. As many RHEA form oxide scales, which grow internally as a result of the inward oxygen diffusion, the PBR is a parameter, which needs to be considered.[25,26,28,43]

3.4. Role of Specific Alloying Elements

Current chemical compositions of RHEA do not vary strongly. Besides the four RM, i.e., Mo, Nb, V, and Ta, the composition of a typical RHEA includes Ti, Cr, Zr, Hf, and Al. Only few RHEA additionally contain Si[30–32,35] or Y.[46] **Table 7** summarizes the key features of these elements and their main impacts on the oxidation resistance. The content of Table 7 was deliberately selected based on 1) the considerations presented earlier in this work and 2) the conclusions made by the corresponding cited authors. Note that the influence of the elements on other properties, such as mechanical properties, density, etc., is not considered in Table 7.

3.5. Oxidation Mechanism of RHEA

The analysis of the oxidation behavior of RHEA investigated so far allows for the conclusion that the oxidation mechanisms can be classified into four categories, which could be generally deduced from the various types of appearance of corrosion products in Figure 4. The oxidation resistance increases continuously from mechanism I to IV as displayed in **Figure 9**. RHEA, which oxidize according to mechanism I, Figure 9a, primarily suffer from severe solubility of oxygen in the metal or alloy causing extensive local crack formation in the oxygen-rich region, which finally leads to partial exfoliation of outer substrate layers. The crack formation in the alloy can be explained by the anisotropic distortion of the surrounding lattice if an interstitial atom occupies an octahedral site in a bcc metal such as Nb or Ta.[3] This

Table 7. Impact of elements relevant for RHEA systems on oxidation resistance.

Element	Positive impact on oxidation behavior	Negative impact on oxidation behavior	Minimum [min] and/or maximum [max] concentrations
Hf	–	Supports pesting by increasing the volume of oxides[25]	Min: 4 at%[32] Max: 20 at%[24]
Mo	–	Volatile MoO_3 above 795 °C[26,27]	Min: 10 at%[21] Max: 33.4 at%[33]
Nb	–	Forms polymorphic oxides[26]	Min: 12.5 at%[25] Max: 30 at%[28]
Ta	Increases the temperature required to form Nb_2O_5[28] $CrTaO_4$ former[2930]	–	Min: 10 at%[21] Max: 33.4 at%[33]
V	–	Volatile V_2O_5 above 678 °C[34,58]	Min: 17.24 at%[34] Max: 25 at%[43]
W	–	Volatile WO_3 above 1000 °C[55]	20 at%[55]
Zr	–	Forms fast growing ZrO_2 Supports pesting by increasing the volume of the oxides[25]	Min: 5.9 at%[58] Max: 25 at%[25,43,57]
Ti	Supports the formation of complex oxides with high solubility of different metal cations[26,34]	–	Min: 5.4 at%[30,31] Max: 37.5 at%[25]
Al	Al_2O_3 former Reduces oxidation kinetics[27]	–	Min: 8.62 at%[34] Max: 35 at%[32]
Cr	Cr_2O_3 and $CrTaO_4$ former[26] Neutralize the presence of Nb_2O_5 by the formation of $NbCrO_4$[43]	–	Min: 10 at%[27] Max: 30 at%[27]
Si	Prevents the formation of V oxides Facilitates the formation of alumina scale[34] Reduces nitridation[30]	–	Min: 1 at%[35] Max: 24 at%[32] –
Y	Improves scale adherence[46]	–	Min: 0.5 at%[46] Max: 1 at%[60]

leads to fast disintegration of significant parts of the outer metal and failure of the oxide scales. The alloy TiZrNbHfTa is believed to be a representative of this oxidation mechanism.[24]

The key feature of oxidation mechanism II, Figure 9b, is the formation and fast growth of oxides that form a mixture of oxides. Such scales are usually highly porous and allow unhampered inward diffusion of oxygen. The diffused oxygen is consumed by oxide growth and oxygen dissolution in the alloy. The oxide scale often has a lamellar structure parallel to the substrate/oxide interface (Figure 4b). Such a lamellar structure may be a result of a repetitive exfoliation of outer layers of the oxygen-rich alloy at the substrate/oxide interface—analogously to mechanism I described earlier. While external scale growth is by far faster (usually linear), internal oxidation/corrosion appears to be rather marginal and proceeds according to the respective diffusion coefficients of oxygen/nitrogen in a corresponding alloy. The alloy NbMoCrTiAl exhibits an oxidation behavior typical of oxidation mechanism II.[26]

According to oxidation mechanism III, Figure 9c, relatively protective oxide scales, e.g., $CrTaO_4$ layers, form at the oxide/metal interface. The reaction between Cr_2O_3 and Ta_2O_5 results in the formation of rutile-type $CrTaO_4$. The crucial benefit of $CrTaO_4$ as compared with, for example, $CrNbO_4$ is that Ta_2O_5—as precursor in the formation of $CrTaO_4$—is stable only as a monoclinic α-Ta_2O_5 up to 1350 °C in contrast to Nb_2O_5 that yields several polymorphic modifications.[44,45] $CrTaO_4$ scales effectively prevent the outward diffusion of metal cations. However, noteworthy internal corrosion zones are often observed, indicating severe inward diffusion of oxygen and/or nitrogen through the scale. Several RHEA, i.e., 3.4Ta20.3Mo15.2Nb25.2Cr5.4Ti17.6Al2.9Si, TaMoCrTiAl, and TaMoCrTi, form such dense, thus, relatively protective $CrTaO_4$ scales.[29,30,33]

Finally, RHEA oxidizing according to mechanism IV, Figure 9d, possess the highest oxidation resistance, as they form dense Al_2O_3 scales (see Figure 4d), which serve as a reliable diffusion barrier layer. Certainly, the high Al content in this alloy seems to be decisive in the formation of a dense alumina scale. It can further by hypothesized that the alumina formation in this alloy is supported by the substantial amounts of Si and Hf, which are known to facilitate the formation of protective oxide layers.[47,48] Such a very protective alumina scale was only observed on the alloy Nb1.3Si2.4Ti2.4Al3.5Hf0.4.[32]

4. Future Research and Development Directions

The RHEA reviewed in this article revealed a broad spectrum of oxidation resistance ranging from the high protectiveness

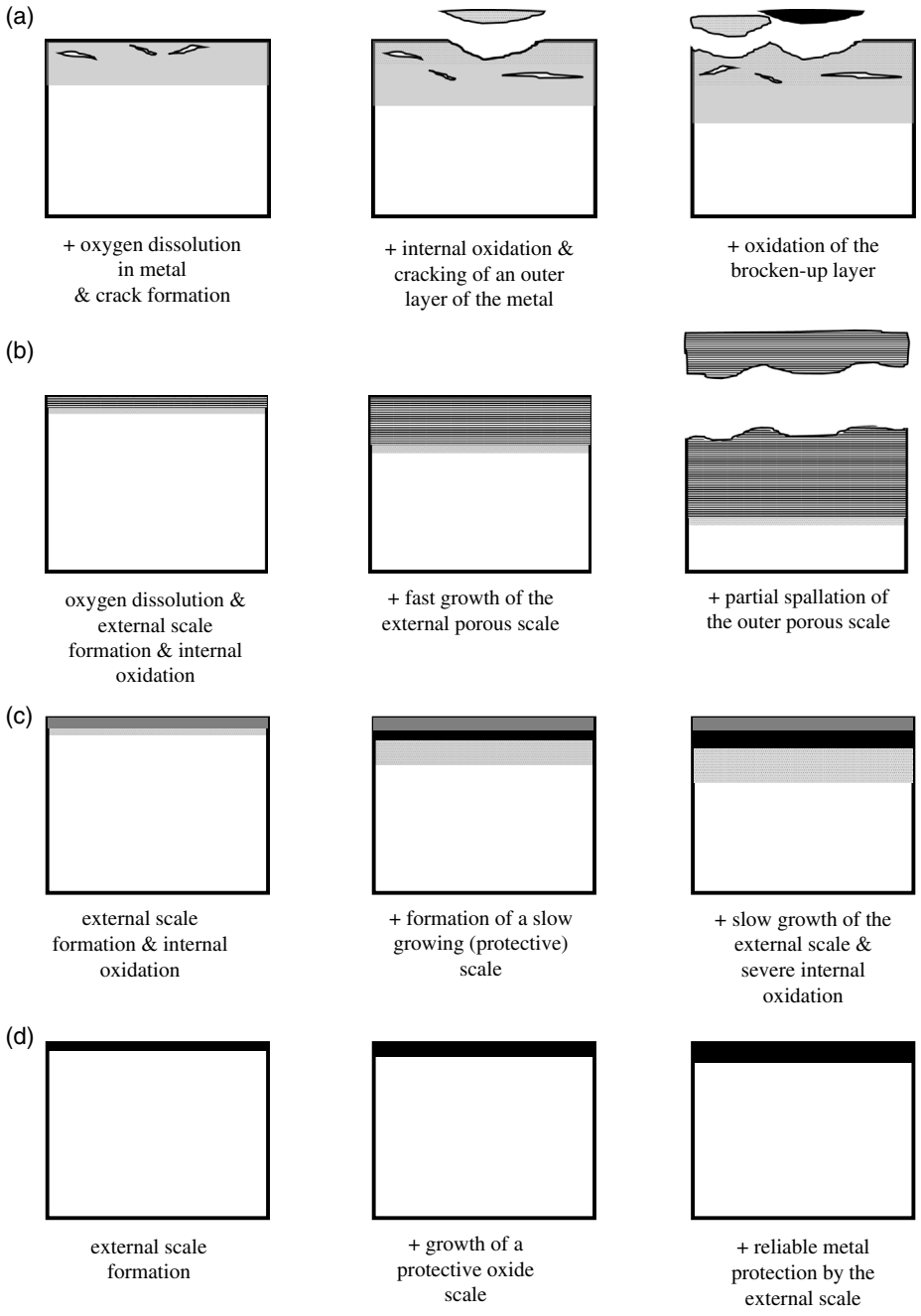

Figure 9. Typical oxidation mechanisms observed in RHEA; a) oxidation mechanism I, b) oxidation mechanism II, c) oxidation mechanism III, and d) oxidation mechanism IV.

due to Al_2O_3 scales to dramatic phenomenon such as pesting. Hence, four major development directions may be pursued in future work.

4.1. Oxidation Experiments and Evaluation of Their Results

The compilation of works reviewed in this manuscript demonstrates that, while most of the investigations were carried out in air, other test conditions such as temperature and duration vary strongly depending on the ability of a particular alloy to resist specific environmental conditions. Therefore, in case of RHEA that possess a relatively high oxidation resistance, long-term, application relevant oxidation tests should be preferred over short-time tests, as the latter may often bring higher degree of uncertainty and lead to false conclusions. However, short-term oxidation experiments are equally indispensable for transient oxidation studies, which enable the fundamental understanding of oxide formation and oxide growth

mechanisms. Often, research activities concentrate on oxidation behavior at very high temperatures neglecting the oxidation resistance at moderate temperature between 500 and 800 °C and, therefore, possible pesting occurrence in RHEA. The testing temperature range should be expanded and, therefore, the pesting temperature regime (if applicable) should be identified. Furthermore, oxidation behavior in atmospheres other than air, such as oxygen-reduced atmospheres as well as complex atmospheric environments, e.g., in combustion engines, should be carried out. Such studies substantially support the identification of relevant oxidation mechanisms. Unfortunately, no such studies have been reported so far. The same holds true for cyclic oxidation experiments, which would also provide essential data for potential future applications. As RM are prone to form volatile oxide species, any weight change results should be critically assessed when oxidation kinetics is concerned. Furthermore, possible substantial uptake of gaseous impurities, especially O and N, and their impact on microstructure evolution needs to be considered when interpreting and discussing the experimental results. Finally, the RHEA community should pay attention on the effect of manufacturing/processing on the alloy microstructure and, subsequently, on the oxidation behavior.

4.2. Al_2O_3-Forming RHEA

As shown earlier, few RHEA form either dense and compact Al_2O_3 scales or at least semi-continuous networks of Al_2O_3 particles demonstrating the intrinsic ability of RHEA to form Al_2O_3 protective scales. These experimental findings should encourage the community to focus their efforts on developing new oxidation resistant Al_2O_3-forming RHEA. If such RHEA consist of brittle phases, e.g., B2 and Laves phase, they may be used as a coating material for alloys, which possess superior mechanical properties but poor oxidation behavior. One should be aware that low melting eutectics (~1200 °C) may form if Al_2O_3 reacts with other oxides such as Nb_2O_5.[49]

4.3. $CrTaO_4$-Forming RHEA

In addition to Al_2O_3-forming alloys, RHEA that form mixed oxides, in particular, $CrTaO_4$ former, should further be investigated. To date, the properties of $CrTaO_4$ are still widely unknown; however, the first screening of $CrTaO_4$-former RHEA shows very promising results, Figure 6. It could be speculated that the protective properties of $CrTaO_4$ may be further improved, applying doping with appropriate reactive elements.

4.4. Alternatives to Protect RHEA

In addition to coatings as a commonly applied method against oxidation and corrosion, alternative approaches, such as aluminizing or surface modification, could be utilized to improve the oxidation behavior. A further alternate solution to increase the oxidation protectiveness of RHEA may be manufacturing of compositionally graded materials in which the chemical composition of outer layers would be adjusted to provide reliable oxidation resistance.

Acknowledgements

This work was conducted under the financial support of Deutsche Forschungsgemeinschaft (DFG) within the framework of grants no. GO2283/3 and HE 1872/33, which is gratefully acknowledged. Part of this work was performed at the Micro- and Nanoanalytics Facility (MNaF) of the University of Siegen.The authors are indebted for the critical reading and constructive suggestions of the reviewers. This article is part of the *Advanced Engineering Materials* Hall of Fame article series, which highlights the work of top scientists in the field of engineering materials.

Open access funding enabled and organized by Projekt DEAL.

Conflict of Interest

The authors declare no conflict of interest.

Keywords

$CrTaO_4$ complex scales, high-temperature materials, oxidation behavior, refractory high entropy alloys, structural applications

Received: September 6, 2020
Revised: February 2, 2021
Published online:

[1] J. H. Perepezko, *Science* **2009**, *326*, 1068.
[2] T. E. Tietz, J. W. Wilson, *Behavior and Properties of Refractory Metals*, Stanford University Press, Stanford, UK **1965**.
[3] P. Kofstad, *High Temperature Oxidation of Metals*, John Wiley & Sons, New York, NY **1966**.
[4] T. Maruyama, K. Yanagihara, *Mater. Sci. Eng.* **1997**, *828*, 239.
[5] J. W. Yeh, Y. L. Chen, S. J. Lin, S. K. Chen, *Mater. Sci. Forum* **2007**, *560*, 1.
[6] S. Telu, A. Patra, M. Sankaranarayana, R. Mitra, S. K. Pabi, *Int. J. Refract. Metals Hard Mater.* **2013**, *36*, 191.
[7] D. G. Liu, L. Zheng, L. M. Luo, X. Zan, J. P. Song, Q. Xu, X. Y. Zhu, Y. C. Wu, *J. Alloys Compd.* **2018**, *765*, 299.
[8] M. P. Brady, P. F. Tortorelli, L. R. Walker, *Mater. High Temperat.* **2000**, *17*, 235.
[9] D.-B. Lee, G. Simkovich, *Oxid. Met.* **1990**, *34*, 13.
[10] Y.-J. Choi, J.-K. Yoon, G.-H. Kim, W.-Y. Yoon, J.-M. Doh, K.-T. Hong, *Corros. Sci.* **2017**, *129*, 102.
[11] B. Predel, *Mo-Si (Molybdenum-Silicon): Datasheet From Landolt-Börnstein – Group IV Physical Chemistry, Volume 5H (Li-Mg - Nd-Zr)* (Ed: O. Madelung), Springer-Verlag Berlin, Heidelberg **1997**.
[12] B. Predel, in *Nb-Si (Niobium-Silicon): Datasheet From Landolt-Börnstein – Group IV Physical Chemistry, Volume 5H (Li-Mg - Nd-Zr)* (Ed: O. Madelung), Springer-Verlag, Berlin **1997**.
[13] B. Predel, in *Si-Ta (Silicon-Tantalum): Datasheet From Landolt-Börnstein – Group IV Physical Chemistry, Volume 5H (Li-Mg - Nd-Zr)* (Ed: O. Madelung), Springer-Verlag Berlin, Heidelberg **1997**.
[14] B. Predel, in *Si-W (Silicon-Tungsten): Datasheet From Landolt-Börnstein – Group IV Physical Chemistry, Volume 5J: (Pu-Re - Zn-Zr)* (Ed: O. Madelung), Springer-Verlag Berlin, Heidelberg **1997**.
[15] M. K. Meyer, M. Akinc, *J. Am. Ceram. Soc.* **1996**, *79*, 938.
[16] C. D. Wirkus, D. R. Wilder, *J. Am. Ceram. Soc.* **1966**, *49*, 173.
[17] P. Berthod, *Oxid. Met.* **2005**, *64*, 235.
[18] S. C. Choi, H. J. Cho, Y. J. Kim, D. B. Lee, *Oxid. Met.* **1996**, *46*, 51.

[19] N. Sukidi, C. C. Koch, C. T. Liu, *Mater. Sci. Eng. A* **1995**, *191*, 223.
[20] C. S. Giggins, F. S. Pettit, *J. Electrochem. Soc.* **1971**, *118*, 1782.
[21] O. N. Senkov, S. V. Senkova, D. M. Dimiduk, C. Woodward, D. B. Miracle, *J. Mater. Sci.* **2012**, *47*, 6522.
[22] M. A. Azim, B. Gorr, H.-J. Christ, M. Heilmaier, U. Koch, M. Engelhard, *Oxid. Met.* **2017**, *87*, 89.
[23] S. Obert, A. Kauffmann, M. Heilmaier, *Acta Mater.* **2020**, *184*, 132.
[24] C.-H. Chang, M. S. Titus, J.-W. Yeh, *Adv. Eng. Mater.* **2018**, *20*, 1700948.
[25] S. Sheikh, M. K. Bijaksana, A. Motallebzadeh, S. Shafeie, A. Lozinko, L. Gan, T.-K. Tsao, U. Klement, D. Canadinc, H. Murakami, S. Guo, *Intermetallics* **2018**, *97*, 58.
[26] F. Müller, B. Gorr, H.-J. Christ, J. Müller, B. Butz, H. Chen, A. Kauffmann, M. Heilmaier, *Corros. Sci.* **2019**, *159*, 108161.
[27] O. A. Waseem, U. Auyeskhan, H. M. Lee, H. J. Ryu, *J. Mater. Res.* **2018**, *33*, 3226.
[28] T. M. Butler, K. J. Chaput, *J. Alloys Compd.* **2019**, *787*, 606.
[29] B. Gorr, F. Müller, S. Schellert, H.-J. Christ, H. Chen, A. Kauffmann, M. Heilmaier, *Corros. Sci.* **2020**, *166*, 108475.
[30] K.-C. Lo, Y.-J. Chang, H. Murakami, J.-W. Yeh, A.-C. Yeh, *Sci. Rep.* **2019**, *9*, 7266.
[31] K.-C. Lo, H. Murakami, J.-W. Yeh, A.-C. Yeh, *Intermetallics* **2020**, *119*, 106711.
[32] M. Ghadyani, C. Utton, P. Tsakiropoulos, *Materials* **2019**, *12*, 759.
[33] L.-C. Li, M.-X. Li, M. Liu, B.-Y. Sun, C. Wang, J.-T. Huo, W.-H. Wang, Y.-H. Liu, *Science China Mater.* **2020**, https://doi.org/10.1007/s40843-020-1332-2.
[34] C. M. Liu, H. M. Wang, S. Q. Zhang, H. B. Tang, A. L. Zhang, *J. Alloys Compd.* **2014**, *583*, 162.
[35] B. Gorr, F. Mueller, H.-J. Christ, T. Mueller, H. Chen, A. Kauffmann, M. Heilmaier, *J. Alloys Compd.* **2016**, *688*, 468.
[36] S. Becker, A. Rahmel, M. Schorr, M. Schütze, *Oxid. Met.* **1992**, *38*, 425.
[37] P. Massard, J. C. Bernier, A. Michel, *J. Solid State Chem.* **1972**, *4*, 269.
[38] K. Hauffe, *Mater. Corros.* **1967**, *18*, 956.
[39] E. A. Gulbransen, K. F. Andrew, F. A. Brassart, *J. Electrochem. Soc.* **1964**, *110*, 952.
[40] J. G. Keller, D. L. Douglass, *Oxid. Met.* **1991**, *36*, 439.
[41] A. Kafri, A. Makonovitsky, R. Z. Shneck, *Defect Diffus. Forum* **2018**, *383*, 133.
[42] F. Klein, T. Wegener, A. Litnovsky, M. Rasinski, X. Tan, J. Schmitz, C. Linsmeier, J. Coenen, H. Du, J. Mayer, U. Breuer, *Metals* **2018**, *8*, 488.
[43] T. M. Butler, K. J. Chaput, J. R. Dietrich, O. N. Senkov, *J. Alloys Compd.* **2017**, *729*, 1004.
[44] J. Spyridelis, P. Delavignette, S. Amelinckx, *Phys. Status Solidi B* **1967**, *19*, 683.
[45] H. Schäfer, R. Gruehn, F. Schulte, *Angew. Chem. Int. Ed. Engl.* **1966**, *5*, 40.
[46] F. Müller, B. Gorr, H.-J. Christ, H. Chen, A. Kauffmann, M. Heilmaier, *Oxid. Met.* **2020**, *94*, 147.
[47] S. Wang, Y. Wu, F. Gesmundo, Y. Niu, *Oxid. Met.* **2008**, *69*, 299.
[48] S. Taniguchi, H. Juso, T. Shibata, *Oxid. Met.* **1998**, *49*, 325.
[49] R. Serrazina, J. S. Dean, I. M. Reaney, L. Pereira, P. M. Vilarinho, A. M. O. R. Senos, *J. Mater. Chem. C* **2019**, *7*, 14334.
[50] M. G. Frohberg, *Thermodynamik Für Werkstoffwissenschaftler, -Ingenieure Und Metallurgen: Eine Einführung*, Wiley-VCH-Verl., Weinheim **2009**.
[51] H. A. Porte, J. G. Schnizlein, R. C. Vogel, D. F. Fischer, *J. Electrochem. Soc.* **1960**, *107*, 506.
[52] B. S. Murty, J.-W. Yeh, S. Ranganathan, P. P. Bhattacharjee, High-Entropy Alloys, Elsevier, San Diego **2019**.
[53] N. M. Geyer, Protection of refractory metals agains atmospheric environmentsDirectorate of Materials and Processes, ASD, **1961**, http://contrails.iit.edu/DigitalCollection/1961/ASDTR61-322article07.pdf. (accessed: September 2020).
[54] A. M. Russell, K. L. Lee, in *Structure-Property Relations in Nonferrous Metals*, John Wiley, Hoboken NJ **2005**.
[55] B. Gorr, F. Müller, M. Azim, H.-J. Christ, T. Müller, H. Chen, A. Kauffmann, M. Heilmaier, *Oxid. Met.* **2017**, *88*, 339.
[56] F. Müller, B. Gorr, H.-J. Christ, H. Chen, A. Kauffmann, M. Heilmaier, *Mater. High Temp.* **2018**, *35*, 168.
[57] J. Jayaraj, P. Thirathipviwat, J. Han, A. Gebert, *Intermetallics* **2018**, *100*, 9.
[58] N. Yurchenko, E. Panina, S. Zherebtsov, G. Salishchev, N. Stepanov, *Materials* **2018**, *11*, 2526.
[59] Y. Xiao, W. Kuang, Y. Xu, L. Wu, W. Gong, J. Qian, Q. Zhang, Y. He, *J. Mater. Res.* **2019**, *34*, 301.
[60] R. Gawel, Ł. Rogal, K. Przybylski, *J. Mater. Eng. Perform.* **2019**, *28*, 4163.
[61] P. Zhang, Y. Li, Z. Chen, J. Zhang, B. Shen, *Vacuum* **2019**, *162*, 20.
[62] S. K. Varma, F. Sanchez, S. Moncayo, C. V. Ramana, *J. Mater. Sci. Technol.* **2020**, *38*, 189.
[63] O. A. Waseem, H. J. Ryu, *J. Alloys Compd.* **2020**, *828*, 154427.
[64] W. D. Klopp, NASA-report TM X-1867, **1969**.
[65] R. P. Elliot, *Trans. AIME* **1954**, *200*, 990.
[66] H. Jehn, E. Olzi, *J. Less Common Met.* **1972**, *27*, 297.
[67] A. U. Seybolt, H. T. Sumsion, *Trans. AIME* **1953**, *179*, 292.
[68] E. Gebhardt, H.-D. Seghezzi, W. Dürrschnabel, *J. Nucl. Mater.* **1961**, *4*, 255.
[69] R. F. Domagala, R. Ruh, *ASM Trans. Q.* **1965**, *58*, 164.
[70] T. H. Schofield, A. E. Bacon, *J. Inst. Met.* **1955-56**, *84*, 47.
[71] M. P. Brady, P. F. Tortorelli, E. A. Payzant, L. R. Walker, *Oxid. Metals* **2004**, *61*, 379.
[72] H. J. Maier, T. Niendorf, R. Bürgel, in *Handbuch Hochtemperatur-Werkstofftechnik: Grundlagen, Werkstoffbeanspruchungen, Hochtemperaturlegierungen Und -Beschichtungen*, Springer Vieweg, Wiesbaden **2019**.
[73] S. D. Cramer, B. S. Covino Jr., *ASM Handbook Volume 13B, Corrosion: Materials*, ASM International, Materials Park, OH **2005**.
[74] N. Birks, G. H. Meier, F. S. Pettit, *Introduction to the High Temperature Oxidation of Metals*, Cambridge University Press, Cambridge **2006**.

Bronislava Gorr, born in 1973, graduated from the National University of Shipbuilding in Mikolaiv, Ukraine with a degree in mechanical engineering, in 1996. After a five-year practical experience as process engineer, she completed her postgraduate studies in mechanical engineering from University Siegen, Germany in 2005, where she also received her Ph.D. (2011) and habilitation (2017). In 2020, she joined the Karlsruhe Institute of Technology (KIT) as a professor for materials for extreme environments. Her research focuses on the development and characterization of high temperature materials.

Steven Schellert, born in 1991, graduated from the University of Siegen, Germany with a degree of Master of Science in 2018. Subsequently, he joined the group for Material Science and Material Testing as a Ph.D. candidate at the same University. His research includes the development and characterization of novel refractory metal-based materials for high temperature structural applications. In particular, he focuses on the thermodynamic modeling and experimental investigations of the oxidation behavior of refractory high entropy alloys.

Franz Müller, born in 1991, graduated with a Master degree in materials science from the University of Siegen in 2016. He subsequently joined the group of Materials Science and Material Testing, where he worked on the development of refractory high entropy alloys for high temperature applications.

Hans-Jürgen Christ, born in 1954, graduated from in 1980. He received a Ph.D. and a habilitation from University of Erlangen-Nürnberg in 1984 and 1990, respectively. After a stay as a visiting professor at the University of Illinois at Urbana-Champaign, he has been a full professor of materials engineering at the University of Siegen, since 1993. His research focuses on the detailed understanding of the behavior of metals and alloys under complex conditions representing those in service of engineering materials. Therefore, correlation of microscopic processes with resulting macroscopic property changes is used to obtain information on the relevant mechanisms and damage processes.

Alexander Kauffmann was awarded doctorate by Faculty of Mechanical Science and Engineering at Dresden University of Technology in 2014. In the same year, he joined Karlsruhe Institute of Technology (KIT) as a postdoc. He is currently group leader of physical metallurgy at Institute for Applied Materials (IAM-WK) and his research interests focus on the development and characterization of metallic and intermetallic materials for extreme conditions including for example low and ultrahigh temperature deformation.

Martin Heilmaier, born in 1962, graduated from University of Erlangen-Nürnberg in 1988. He received a Ph.D. degree from University of Erlangen-Nürnberg in 1992. After postdoctoral stays at IFW Dresden and UWA in Perth, he was a team leader R&D of Refractory Metals at Plansee SE, Reutte/Austria. After full professor positions at Otto-von-Guericke-University Magdeburg (2002–2008) and TU Darmstadt (2008–2011), he currently holds the Chair for Materials Science & Engineering at the Institute for Applied Materials, Karlsruhe Institute of Technology. His research areas include the development of novel high temperature structural materials, intermetallic compounds, high entropy alloys, and their mechanical testing under extreme environmental conditions.